JOM, Vol. 67, No. 5, 2015
DOI: 10.1007/s11837-015-1292-0

Corrosion Fatigue Behavior of 316LN SS in Acidified Sodium Chloride Solution at Applied Potential

A. POONGUZHALI,[1] M.G. PUJAR,[1,2,3] C. MALLIKA,[1] and U. KAMACHI MUDALI[1]

1.—Corrosion Science and Technology Group, Indira Gandhi Centre for Atomic Research, Kalpakkam 603102, India. 2.—e-mail: pujar55@gmail.com. 3.—e-mail: pujar@igcar.gov.in

The influence of acidified 1 M NaCl solution by addition of 2 ml/L of HCl on the cyclic plastic deformation of AISI Type 316LN SS containing 0.07 wt.% and 0.22 wt.% N was investigated as a function of the applied potentials. The corrosion fatigue (CF) behavior of stainless steel (SS) was explained vis-a-vis the dislocation behavior, the propensity to form microcracks, and the evolution of the current transients based on the studies carried out at both room-temperature and boiling conditions. CF experiments were conducted using round tensile specimens at a stress ratio of 0.5 and a frequency of 0.1 Hz. Two different kinds of damage mechanisms were observed (I) the damage mechanism in the stable–passive state was correlated with the localization of the anodic dissolution due to a depassivation–repassivation process, whereas (II) the cyclic stress induced pitting corrosion in the metastable pitting state, which resulted in formation of microcracks. The study of the microcracking process and its evolution is a key to the physical mechanism by which the fatigue life of stainless steels would be affected in an aqueous corrosive solution under the applied potential.

INTRODUCTION

High-nitrogen steels (HNS) and nitrogen-bearing stainless steels (SS) are becoming an important class of engineering materials for various applications in power plants, refineries, chemical process plants, and more.[1] The addition of nitrogen in these alloys is known to have several beneficial effects, including improvements in phase stability, strengthening, and corrosion resistance. Nitrogen additions have been widely reported to have a beneficial effect on the pitting and crevice corrosion resistance of Fe-Cr-Ni-Mo steels in acidic-chloride environments.[2–4] For the structural components of the prototype fast breeder reactor (PFBR) under construction at Kalpakkam in India, low-carbon austenitic stainless steel alloyed with 0.06–0.08 wt.% nitrogen has been selected as the major structural component.[5] Although literature reports on environmental degradation processes such as stress corrosion cracking (SCC) and corrosion fatigue (CF) are available for these SS, adequate information on long-term CF strength and mechanism of CF crack initiation is not available for these SS. Most of the CF failures of machine components and structures reported that CF cracks initiated from corrosion pits.[6,7] Pitting corrosion is influenced by different parameters, including the environment, metal/alloy composition, potential, temperature, and surface condition/finish. Environmental parameters include aggressive ion concentration, presence or absence of dissolved oxygen, pH, and inhibitor concentration. Other phenomenological aspects of localized corrosion involve the stochastic nature of the processes and the stages of localized attack, including passive film breakdown and metastable pitting attack.[8,9] Stainless steels suffer from localized corrosion when in contact with corrosive environments like chloride solutions. Passive film breakdown followed by pit initiation have been discussed through three main steps, which include passive film penetration, film breaking, and adsorption.[10]

A corrosive environment can lead to a marked reduction in fatigue resistance as well as to the elimination of the fatigue limit. In the early stage of CF process, corrosion pits are initiated, which grow deeper, and a final failure of the specimen results by crack initiation and propagation from the grown

(Published online January 29, 2015)

pits even if the applied stress amplitudes are smaller.[11] When coupled with fatigue, pitting corrosion damage acts as a stress raiser and moves the endurance of the metal from the domain of crack initiation to the domain of life reduction by crack propagation. Fatigue cracks in SS were shown to be initiated at the corrosion pits and in 12% Cr high-strength martensitic alloys where the crack initiation time represented most of the fatigue life.[12] Shalaby et al.[13] found that crack initiation in these steels was environmentally controlled in chloride solutions and occurred at pits, sites of dissolved nonmetallic inclusions, and areas of etched grain boundaries formed during the fatigue tests. In 316L SS, crack initiation was related to the formation of both pitting and intergranular corrosion (IGC).[14,15] Grain boundaries were shown to be attacked preferentially within the pits, forming stress-raising notches which then became crack initiation sites. As the crack propagated, it transformed from the initial intergranular form to a transgranular mode. The reduction of fatigue resistance in the presence of an aqueous solution is generally associated with a local interaction between a mechanical and an electrochemical damage. During CF, the localization of the plastic strain due to fatigue can enhance localized corrosion damage, which may be described in terms of dissolution and/or hydrogen-reduction reactions. The corrosion damage can favor the localization of the cyclic strain as well as the electrochemical potential that governs the kinetics of the corrosion reactions.[16]

Although localized corrosion damage is known to be the initiation site for fatigue cracks, factors controlling the transformation of flaws into cracks are not yet understood. Considering the chemical variables affecting pitting corrosion resistance, the temperature of electrolyte medium encountered by the materials during service plays a major role. An increase in electrolyte temperature would significantly affect the stability of the passive film and activate the pitting kinetics leading to decrease in the pitting corrosion resistance.[17] The distribution of alloying elements across the passive film and their chemical state significantly affects the stability of the film against localized corrosion attack.[18] The overall mechanisms involved in the breakdown of passivity are associated with chemical breakdown, which leads to localized corrosion by damaging species like Cl^- or the higher atomic weight halides. Second, the mechanical breakdown of passivity results from the application of externally applied stress. Okamoto[19] and Fromhold[20] explained the sudden current and potential transients in terms of a crack/heal mechanism at the base of the flaws or defects caused by the combined action of compressive and/or tensile stresses present in the air-formed oxide, which expose bare metal transiently to the electrolyte. The relief of these stresses is expected to occur at the flaws in the oxide film, where the film is thinner and weakened leading to its easy dissolution.[21] This article describes a study of the influence of pitting corrosion in SS on the initiation and early growth of fatigue cracks. The main objective of this article is to analyze the CF mechanism in AISI type 316LN SS with 0.07 wt.% and 0.22 wt.% of nitrogen in acidified 1 M NaCl solution. High-cycle fatigue tests at an imposed mean stress of 375 MPa were carried out to evaluate the dislocation behavior as well as the evolution of the corrosion current transients at applied potentials in the domains of (I) passivity and (II) metastable pitting.

EXPERIMENTAL PROCEDURE

Two commercial heats of 316LN SS, containing 0.07 wt.% and 0.22 wt.% nitrogen, were used. The chemical composition of the two heats of 316LN SS and their grain sizes are given in Table I. The hot-rolled plates of 25 mm thick were solution annealed at 1323–1423 K for 1 h followed by water quenching. The plates were then pickled and passivated.

Electrochemical Polarization Behavior

Potentiodynamic anodic polarization experiments were conducted on the round tensile specimens of AISI Type 316LN SS, which were ground up to 1200 grit in the gauge length. These experiments were conducted at room temperature and boiling conditions of the solution to obtain the applied potential behavior of the specimen. The tests were carried out in air-saturated 1 M NaCl solution acidified to a pH of 1.6 by the addition of 2 ml/L HCl. The potentials were measured against a saturated calomel electrode (SCE). Two platinum foils of about 1 cm^2 area were spot welded to platinum wires and were used as counter or auxiliary electrodes. Then, they were placed around the working electrode (WE) symmetrically for uniform current distribution. The potential scan rate was 10 mV/min and the potentiodynamic polarization experiment was started from 200 mV active to the stable open circuit potential (OCP), which was measured after 1 h immersion of the specimen in the solution. The

Table I. Chemical composition of AISI Type 316LN SS (wt.%)

Specimen designation	N	C	Mn	Cr	Mo	Ni	Si	S	P	Fe	Average grain size (μm)
7 N	0.07	0.027	1.7	17.53	2.49	12.2	0.22	0.006	0.013	Bal	87.3
22 N	0.22	0.028	1.70	17.57	2.54	12.36	0.20	0.006	0.018	Bal	86.8

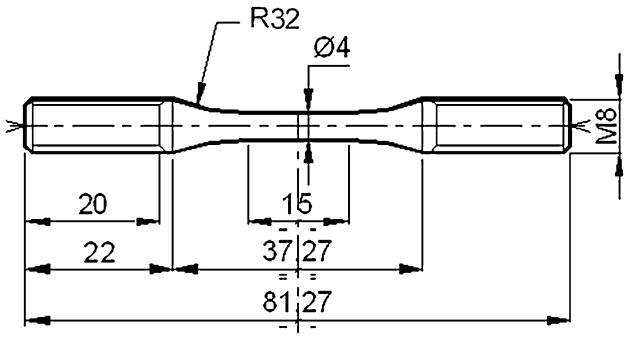

Fig. 1. A schematic of the round tension specimen.

potential was scanned in the anodic direction until the specimen underwent stable pitting, which was signified by the monotonic rise in the current after the passive potential range. The potentiodynamic anodic polarization diagrams were plotted from the current, potential data to know the range of passivity and passive current density (I_{pass}).

Corrosion Fatigue Studies

Round tension specimens were fabricated for CF studies from the solution-annealed plates of AISI Type 316LN SS with two different nitrogen contents. The schematic of the specimens is given in Fig. 1. Corrosion fatigue tests were carried out under load control mode using a Zwick Roell (ROELL AMSLER Dynamic Testing GmbH & Co. KG. Gottmadingen, Germany) servo hydraulic system of 25 kN capacity in boiling aqueous solution of 1 M NaCl + 2 ml/L HCl (b.p = 381.5 K; pH 1.56) at a stress ratio of 0.5 and a frequency of 0.1 Hz. Except the region of interest in the gauge length, the rest of the specimen and the specimen train were masked with silicone elastomer. Care was taken to avoid crevice formation between the specimen and the elastomer. The number of cycles to total failure was used as the assessment criterion for determining the susceptibility to CF.

Corrosion Fatigue Studies at Applied Potentials

The specimen undergoing a CF test was polarized at a preset potential (measured against a SCE) using a potentiostat (Model 1287 SI; Solartron), and the resultant current was recorded at 0.1 Hz sampling frequency using Corrware software. The CF behavior of AISI Type 316LN SS with 0.07 wt.% and 0.22 wt.% N was studied in acidified 1 M NaCl as a function of the applied potential in both room-temperature as well as boiling conditions. The CF studies were carried out at applied potentials in the (I) passive region and (II) metastable pitting corrosion region and the current transients were recorded as a function of the applied mean stress of 375 MPa as well as the number of cycles to failure.

Fractography

The fractured surfaces of the failed specimens after the CF tests were examined using a scanning electron microscope (SEM) to study the cracking mode.

RESULTS AND DISCUSSION

Electrochemical Polarization Behavior

The potentiodynamic anodic polarization diagrams of 316LN SS containing two different amounts of nitrogen in acidified 1 M NaCl solution at both room-temperature and boiling conditions are shown in Fig. 2a and b.

The potentiodynamic anodic polarization curve of 316LN SS with 0.07 wt.% nitrogen showed a typical active–passive behavior in acidified 1 M NaCl solution. The passive potential region showed numerous current fluctuations in the range of about 0.2–3 μA, which signify metastable pit nucleation events. The amplitudes of these current fluctuations remained the same until the specimen started to undergo stable pitting at 150 mV (SCE). After pitting potential (E_{pp}), the current rose monotonically. However, the anodic polarization diagram for the specimen in the boiling solution showed completely different features. Although the OCP values of the specimens in the room-temperature as well as boiling solutions were almost comparable, the specimen in the boiling solution showed a continuous rise in the current after OCP without attaining any passivity. Unlike the room-temperature study, no distinct-active peak was obtained in the boiling solution; the specimen showed pseudo-passivity with very high passive current density values. Numerous current transients observed in the room-temperature curve in the passive region suggested formation and repassivation of metastable pits. However, in the high-temperature curve, these were completely absent. The depassivating ability of H^+ ions along with the presence of Cl^- ions breaks down the passive film, resulting in the higher passive currents. From this result, it can be surmised that application of even the passive potential would result in accelerated dissolution of the alloy due to boiling condition. Temperature also favors the kinetics of the corrosion reactions, especially the anodic dissolution of the metal, because the anodic current densities are higher as the temperature increases.[22]

The room-temperature potentiodynamic anodic polarization curve for 0.22 wt.% nitrogen-containing alloy showed typical active–passive behavior with an extended passive region (~750 mV), which was punctuated with innumerable current transients signifying initiation and repassivation of metastable pits. The high-temperature polarization curve for this alloy showed interesting features. Although the range of passivity had decreased drastically (~200 mV), the passive current density

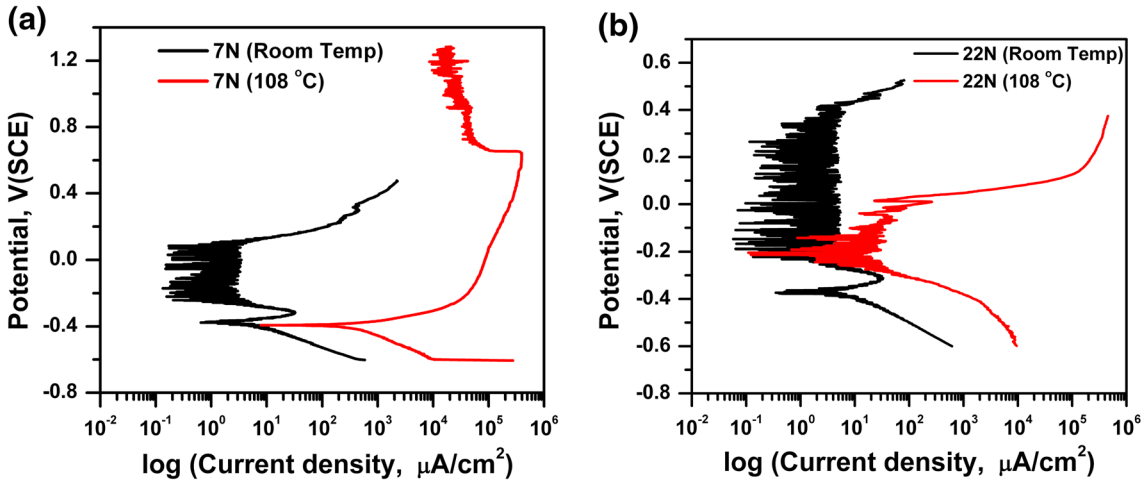

Fig. 2. Potentiodynamic anodic polarization curves for Type 316LN SS containing (a) 0.07 wt.% and (b) 0.22 wt.% nitrogen at both room-temperature and boiling conditions.

values were four orders of magnitude lower than those observed in 0.07 wt.% N steel in the boiling condition. Also, the E_{pp} value at 108°C for the steel with 0.22 wt.% N was nearly within the range to the steel with 0.07 wt.% N at room temperature. Although chloride ions were strongly chemisorbed on the passive film with increase in temperature, increased nitrogen content also strengthened the passive film. This could be due to segregation of nitrogen at the passive film/metal interface, thereby resisting dissolution of the passive film. The chromium-nitrogen steel composition favors the passivation process as well as the longer induction time for pits initiation[23] and nitrogen incorporation in the passive film and formation of a more compact structure. Tzaneva[24] explained the difficulty in anodic dissolution of the bare metal due to nitrogen enrichment of the passive layer or the accumulation of nitrogen on the metal/oxide interface.[25–28] Thus, it was obvious that increased nitrogen addition had resulted in the increased stability of the passive film, which resisted dissolution and early breakdown. Unlike 0.07 wt.% N steel, 0.22 wt.% N steel clearly showed the pitting potential to be about 0.0 V (SCE), and the current rose drastically after E_{pp}.

Effect of Applied Potential

For the CF studies at the applied potential in the passive and metastable pitting regions, based on the polarization curves shown in Fig. 2a and b, the potentials were selected as −0.1 V (SCE) and 0.05 V (SCE), respectively, for both steels. The experimental arrangement for CF studies has been already described. As soon as the solution started to boil, the specimen was polarized potentiostatically at the required potential through the waveguide and cyclic load was applied simultaneously; the specimen remained under applied potential until final failure.

CF Studies in Passive Region: −0.1 V

Figure 3 shows the effect of temperature on the CF behavior of 0.07 wt.% steel due to applied potential in the passive range (−0.1 V (SCE)). In the stable–passive region, the damage mechanism is related to the dynamic depassivation–repassivation process. The specimen showed a lot of current fluctuations at both room-temperature and boiling conditions because of the dynamic depassivation–repassivation process. The passive current in the boiling condition was found to be higher by about two orders of magnitude, which could be attributed to the temperature effect; [29] temperature aids in the dissolution process of the surface due to the presence of an acidic chloride environment. The room-temperature specimen showed high fluctuations with an intermittent rise in current until final failure. The current fluctuations appeared in bunches wherein each bunch showed increased current amplitude compared with the previous one. Between two bunches of current amplitudes, there appeared a current region that reflected repassivation process of the alloy. After 45,000 cycles, the room-temperature specimen showed a drastic decrease in the current amplitude, indicating restricted dissolution in the propagating microcracks.

The specimen in the boiling condition showed current fluctuations in spurts (Fig. 3b). The alloy with 0.22 wt.% nitrogen showed interesting features (Fig. 4a). It was observed that the current amplitude fluctuations linearly increased with increase in the number of cycles, and just before the final failure there was a sudden drop in the current amplitude (after ~96,000 cycles), suggesting rapid failure due to faster crack propagation. Cyclic load was applied with a frequency of 0.1 Hz; however, the process of passivation was much slower than that, thus, the repassivation process of the passive film at the damaged site due to application of the previous cycle could not be completed when the next cycle

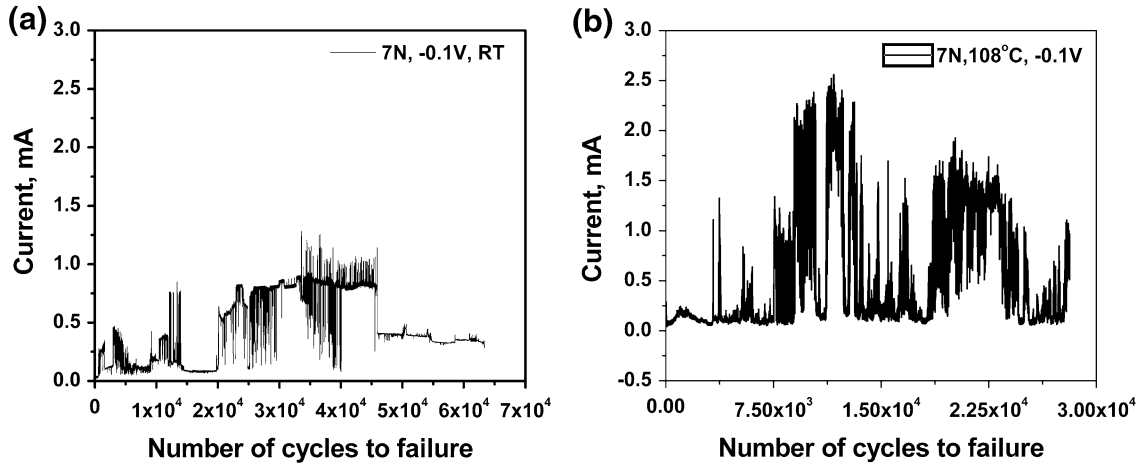

Fig. 3. Variation of current with number of cycles to failure recorded during the CF test of Type 316LN SS with 0.07 wt.% nitrogen at the applied potential of −0.1 V (SCE) for a mean stress of 375 MPa at (a) room-temperature and (b) boiling conditions.

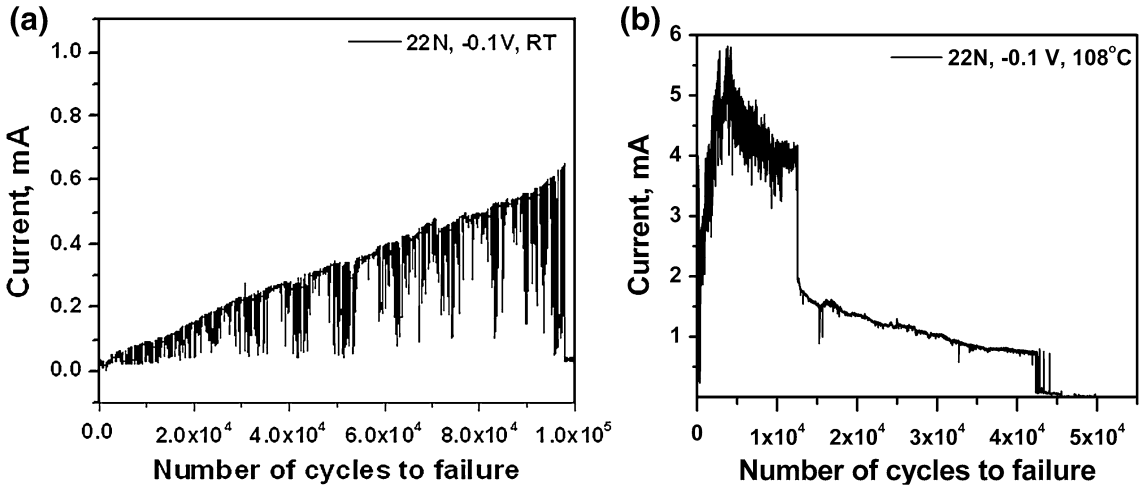

Fig. 4. Variation of current with number of cycles to failure recorded during the CF test of Type 316LN SS with 0.22 wt.% nitrogen at the applied potential of −0.1 V (SCE) for a mean stress of 375 MPa at both room-temperature and boiling conditions.

initiated additional damage to it. Thus, the linear rise in the current amplitude could be attributed to the cumulative damage to the passive film; however, increased nitrogen content facilitated this damage to be always under control with increased passivability by nitrogen addition. In the boiling condition (Fig. 4b), the drop in the current amplitude was at 12,000 cycles and showed the first sign of microcracking. At 42,000 cycles, there was an accelerated cracking process leading to failure. Thus, the temperature effect was obvious at the boiling condition, which led to failure at almost half the cycles needed to fail the specimen during the room-temperature test.

In general, the mechanism of true CF is attributed to the dynamic interaction between the environment and the exposed metal surface undergoing plastic strain. Hence, the effect of strain was studied under a similar applied potential condition as shown in Figs. 5 and 6. Strain displacement for 0.07 wt.% nitrogen SS was generally found to be higher at the outset of the application of the cyclic load at room temperature as well as in the boiling condition, the latter showing a higher value than the former (Fig. 5). However, the strain displacement for 0.22 wt.% nitrogen SS increased gradually as could be seen in Fig. 6, with occasional transient, until final failure, a behavior that closely matches the current amplitude rise observed in Fig. 4. From these trends, it appeared that the damage to the passive film was relatively easier in 0.07 wt.% nitrogen SS than that in 0.22 wt.% nitrogen SS, where resistance to the damage of the passive film was observed and the damage was cumulative until final failure. Thus, an increase in the nitrogen content showed a strengthening effect on the passive film, which resisted rupture under applied cyclic load. The beneficial effect of nitrogen on improved corrosion resistance of austenitic SS is

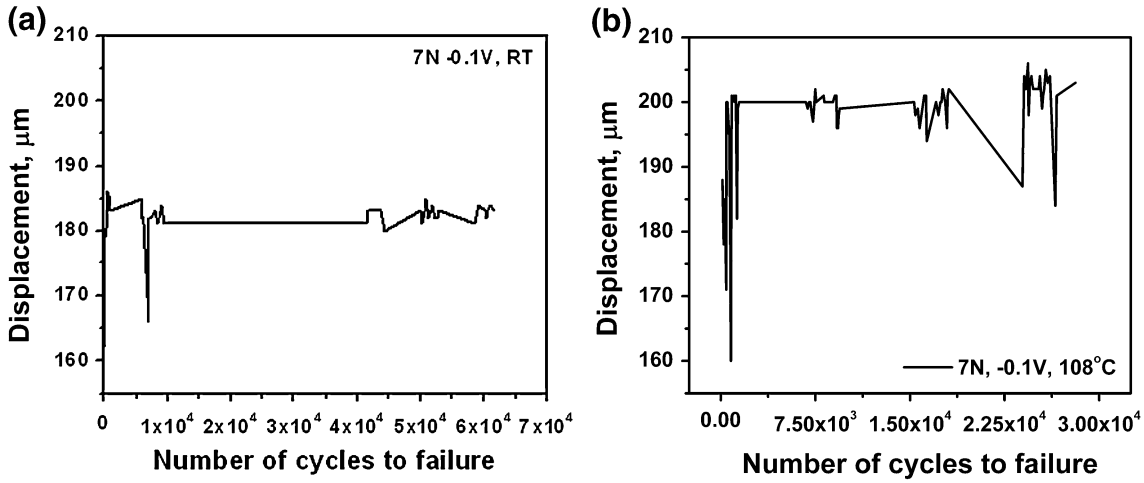

Fig. 5. Variation of strain displacement versusnumber of cycles to failure recorded during the CF test of Type 316LN SS with 0.07 wt.% nitrogen at the applied potential of −0.1 V at both room-temperature and boiling conditions.

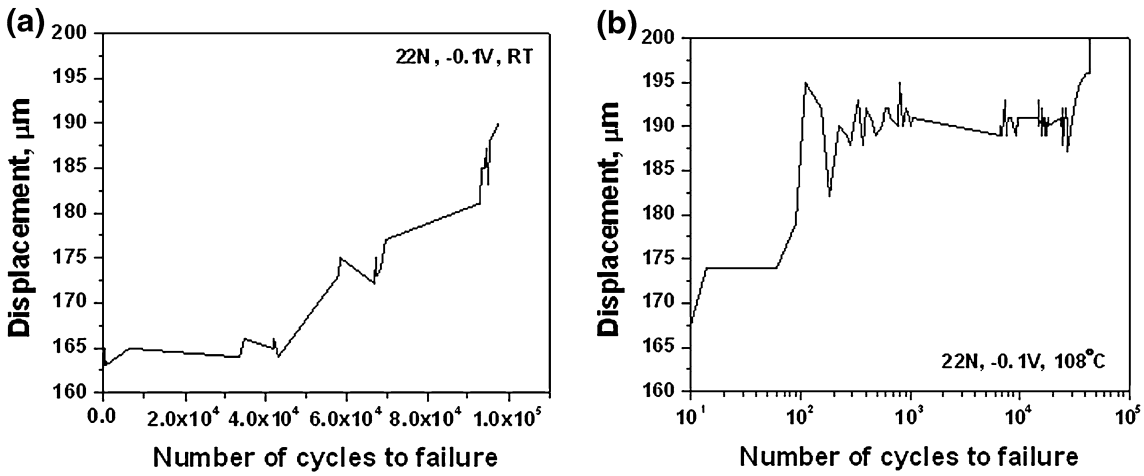

Fig. 6. Variation of strain displacement versus number of cycles to failure recorded during the CF test of Type 316LN SS with 0.22 wt.% nitrogen at the applied potential of −0.1 V at both room-temperature and boiling conditions.

attributed to improved passivity. The mechanisms proposed to explain improved passive film stability due to nitrogen include the formation of ammonium ions [30,31] or nitrate/nitrite ions, nitrogen enrichment on the surface, segregation of nitrogen to anodically dissolving surface, and existence of nitrogen as Cr–N at the metal surface as a complex of ammonia as NO or as an ammonium salt.[32] Mudali and Katada [33] reported that preferential enrichment of nitrogen after active dissolution, leading to blocking of iron atoms from further dissolution. The role of nitrogen is very significant in affecting the propagation of pits as the repassivation of the pits is enhanced by the formation of ammonium as well as nitrate ion formation. Tong et al.[34] indicated that under anodic polarization conditions, the crack tip anodic dissolution current density (during cyclic loading) was three orders of magnitude greater than the general dissolution current density in the absence of applied load for mild steel in a 3.5% NaCI solution. Anodic dissolution at applied anodic potentials may occur not only at the crack tip but also at the nearby crack edges. Consequently, a blunted crack tip rather than a sharp one is developed, resulting in crack branching as discussed later in fractography section. As a result, the crack propagation rate was found to be lower at this potential than the metastable pitting region.[35]

Degallaix et al.[36] attributed the improved fatigue resistance of the nitrogen-dissolved steels to the lengthening of the initiation stage, due to more planar slip and to a more homogeneous deformation through dislocation–solute interactions and/or decrease in stacking fault energy. An increase in the amount of planar slip increased the resistance to strain localization; it made the formation of persistent slip bands more difficult and promoted greater slip reversibility, either of which would retard crack

initiation.[37] The effect of the corrosive environment is mainly associated with an acceleration of the microcrack propagation of Type I cracks on the surface, which are more numerous than those observed in the absence of corrosive environment. The displacement curve did not show a significant rise until final failure. This observation indicates that the effect of environment was less pronounced in the passive state.

CF Studies in Metastable Pitting Corrosion Region: 0.05 V (SCE)

Figure 7a and b show the plots of current in μA as a function of the number of cycles under applied potential in the metastable pitting range [0.05 V (SCE)] for 0.07 wt.% nitrogen steel in both conditions. The room-temperature specimen showed extremely low current fluctuations compared with the specimen in the boiling condition, which is attributed to the high passive currents observed during polarization. Due to the application of the cyclic load, the formation of small current transients were observed, which indicate the formation of metastable pits and their repeated repassivation. However, the current transients continued to remain in the passive region despite repeated depassivation and repassivation cycles. The current in the boiling condition was found to be four orders higher than that in the room-temperature experiment. Because the passive film was already damaged due to the effect of the boiling solution, the effect of cycling loading was obvious through the repeated bunch of current transients, which appeared to be somewhat periodic in nature. By raising the dissolution rate or by making the oxide film thinner, the barriers to slip are reduced; slip localization is favored either by increasing the concentration of anions or by increasing the temperature of the corrosive medium.[38] On average, 40-mA current transients were recorded during the experiment in the boiling condition, which is higher and attributed to the destruction of the passive film and enhanced dissolution of the surface by cyclic loading. The current transients were plotted as a function of time (Fig. 7c) for both conditions. It was observed that the current transients appeared to be fluctuating about a mean value symmetrically after 1 h. These types of current fluctuations are indicative of the formation of metastable pits.[39] Anita et al.[40] reported potential fluctuations of the stressed 316 SS electrode immersed in acidic chloride medium, and they attributed these events to the formation of stable pits. However, in the present case, because the current fluctuations are in the range of μA, metastable pits could have initiated. Although the amplitude of current fluctuations is not high, continuous depassivation and repassivation of the passive film would eventually weaken it, resulting in the formation of metastable pits. It was reported that when steels were cyclically deformed, the passive film could be locally perturbed by cyclic modifications of the topography of the underlying metal. Under these conditions, the fatigue resistance of the SS largely depends on the respective kinetics of mechanical depassivation and electrochemical repassivation.[41] Passive metals such as SS suffer from localized corrosion when in contact with corrosive environments like chloride solutions. When coupled with fatigue, the major part of the total time required for the failure is consumed mainly by the process of initiation of localized corrosion.

The number of cycles to failure in the room-temperature test was 20,000, whereas in the boiling solution, this number drastically decreased to 1200. Temperature can affect the corrosion behavior of materials in different ways and it is well known that pit initiation is hastened due to increase in the solution temperature. Increase in temperatures leads to a decrease in the passive region of the metal and shifts the breakdown potential (E_b) toward the active direction. Most of the chemical and electrochemical reactions proceed more rapidly at higher temperatures. Therefore, the rate of pitting would increase as the temperature increases. Processes accompanying pitting are active dissolution of metal or alloy, dissolution of the oxide film, diffusion of various species through the oxide film into and out of the pit, and formation of salt layer at the bottom of the pit. The rate of the above reactions increases with temperature. Thus, as the diffusion of chloride ions through the passive film increases, the pitting susceptibility of the alloy increases. From Fig. 7b, it is clear that the high current amplitude values in the boiling condition are due to extensive pitting corrosion. The current amplitudes were about five order of magnitude higher than those observed in the specimen anodically polarized at room temperature. During the polarization studies in the boiling condition, extensive removal of corrosion deposits could be observed, which correlates well with the high current amplitudes observed in Fig. 7b. A similar phenomenon was observed in the case of specimen with 0.22 wt.% nitrogen, which showed several current transients as a function of increase in the number of cycles. At about 1500 cycles, the current transients showed a large fluctuation in the amplitude, which indicated breakdown and repassivation of the passive film for the CF experiment conducted at room temperature. This trend, showing an upward rise, continued for a major part of the experiment and then there was a sudden drop in the current amplitude, which signified the onset of a crack at the metastable pit (Fig. 8a). Subsequent to this, the current amplitude showed a downward trend, signifying increased crack propagation until the final failure of the specimen. The 0.22 wt.% nitrogen SS specimen in the boiling condition showed an initial decrease in the current amplitude (Fig. 8b), which was attributed to the strengthening of the passive film formed over the surface, where

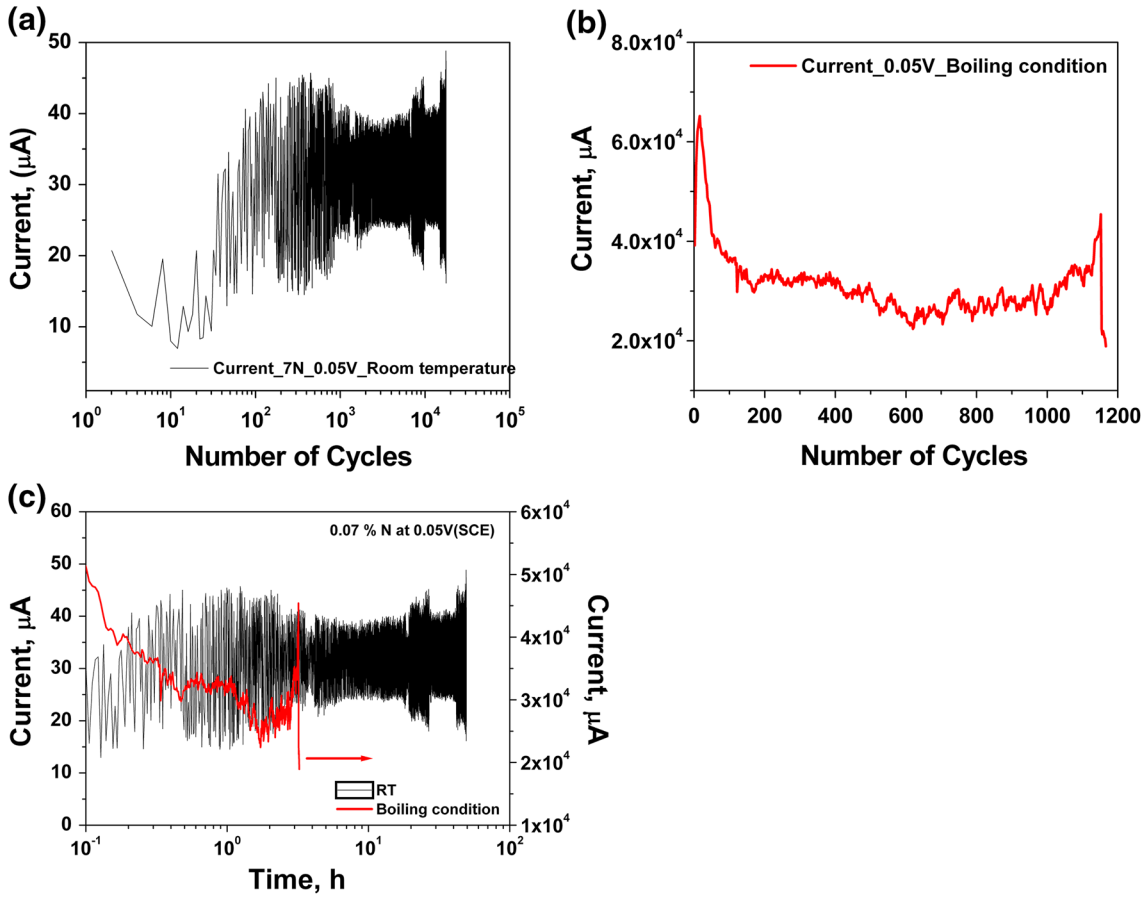

Fig. 7. Variation of current with number of cycles to failure recorded during the CF test at 0.05 V (SCE) for 0.07 wt.% nitrogen steel and at a mean stress of 375 MPa at (a) room-temperature and (b) boiling conditions; (c) current transient plot as a function of time.

the effect of cyclic stress had not yet damaged the film. Thus, the current showed a lower value that remained so for a little more than 6000 cycles; thereafter, the crack initiation at the metastable pits raised the current amplitude drastically until final failure. The crack initiated at the bottom of corrosion pit where stress concentration is large and is presumably electrochemically active.[42] Because of the large number of these corrosion pits and the effectiveness of these pits as stress concentration sites during fatigue, multiple fatigue cracks initiated from these pits are commonly observed; this phenomenon has been discussed later in the Fractography section in detail.

It was observed from Figs. 9a and 10a that in the room-temperature condition, the strain displacement remained constant up to 7.5% 10^3 cycles for 0.07% nitrogen alloy and 17.5% 10^3 cycles for 0.22% nitrogen alloy and thereafter, there was an increase in the displacement owing to crack initiation in the specimens. For the specimen in the boiling condition, strain displacement was much higher, which continuously fluctuated during cyclic loading. This could be attributed to the increased dissolution of passive film at localized sites initiating pits, which resulted in increased displacement. The ability of the material to repassivate even in the boiling condition resulted in fluctuations in the strain displacement. A sharp increase in the displacement was observed in Figs. 9b and 10b beyond 600 cycles and 3×10^3 cycles for 0.07% N and 0.22% N alloy specimens, indicating the formation of microcracks in the specimen in the boiling condition. There are a number of similarities and differences between the mechanisms of crack propagation and those of crack initiation. As in the case of initiation, the processes of oxide or film growth, passivation, and diffusion, and their overall effect on the near-surface dislocation arrangement and local mechanical properties, must be considered. In contrast to crack initiation, however, the site of the chemical–mechanical interaction is restricted to the crack-tip region where the local strains are much higher than those in the persistent slip band. During cyclic stressing, fresh metal surface is constantly being exposed at the crack tip, so that transient oxidation or passivation effects of the order of milliseconds become very important. The surface area exposed is related to the crack-tip opening displacement, which can be as small as a few hundred angstroms. The local chemistry near the crack tip is quite different from that in the bulk of the corrosive solution and hence

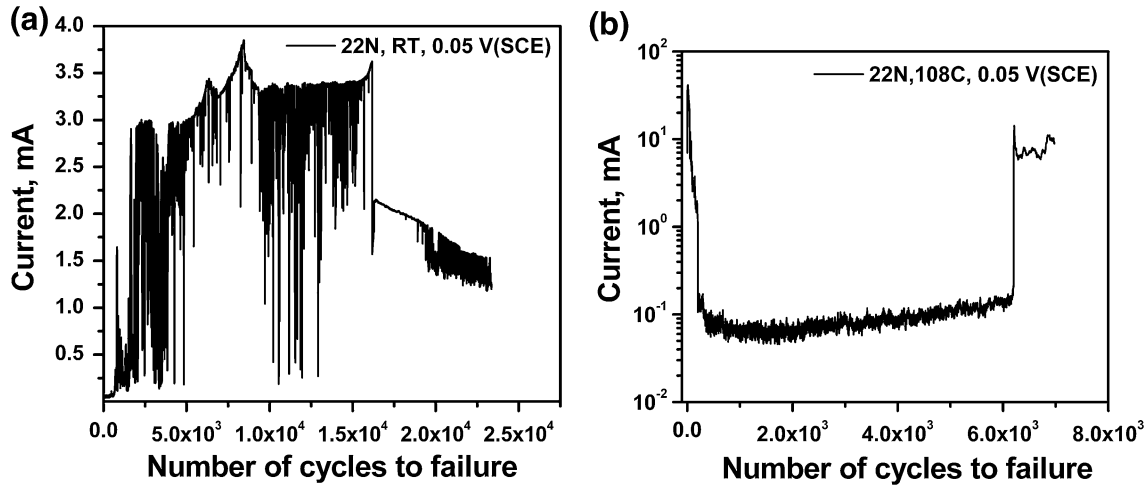

Fig. 8. Variation of current with number of cycles to failure recorded during the CF test of Type 316LN SS with 0.22 wt.% nitrogen at the applied potential of 0.05 V (SCE) for a mean stress of 375 MPa at both (a) room-temperature and (b) boiling conditions.

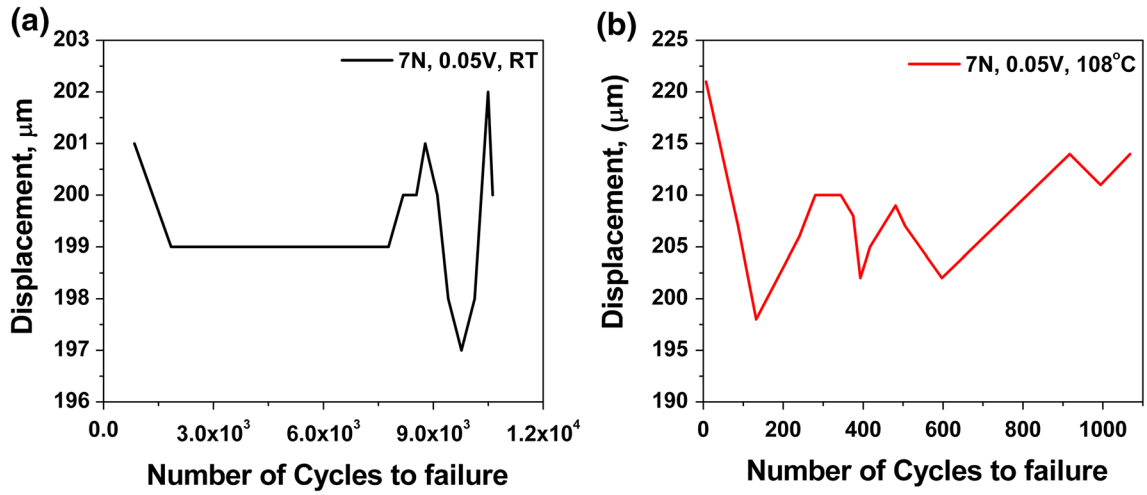

Fig. 9. Variation of strain displacement with number of cycles to failure recorded during the CF test of Type 316LN SS with 0.07 wt.% nitrogen at the applied potential of 0.05 V (SCE) for a mean stress of 375 MPa at both (a) room-temperature and (b) boiling conditions.

the interpretation of externally measured corrosion parameters is difficult. The environment changes the nature of the oxide layer from ductile to brittle. During straining, microcrack formation leads to an increase in local stress concentration and a mechanical increase in crack growth rate.[38] Greenfield[43] considered that environmental interactions by nature are surface interactions; therefore, the aforementioned near-surface dislocation phenomena were strongly affected by the environment.

The study of the microcracking process and its evolution is a key in describing the physical mechanism by which a corrosive medium can affect the fatigue life of SS due to the applied potential. The effect of applied potential in the metastable pitting corrosion region at room temperature clearly depicts the microcrack formation at 7.5×10^3 cycles and 17.5×10^3 cycles for 0.07% and 0.22% N alloys cycles, respectively. Variations were observed in the plots of displacement as well current transients as seen in Figs. 11 and 12 for 316LN SS with 0.07 wt.% and 0.22 wt.% nitrogen at both room temperature and boiling conditions. Both the curves coincided well around 7700 cycles in 0.07 wt% nitrogen, where fluctuations in the current amplitude matched with the strain displacement indicating the opening (resulting in the dissolution of SS and rise in the current amplitude) and closing (resulting in the repassivation and drop in the current amplitude) of the microcracks; this process continued until final fracture of the specimen. However, in the boiling condition, the fluctuations in the strain displacement started much earlier, at a little more than 100 cycles, and they continued until about 600 cycles.

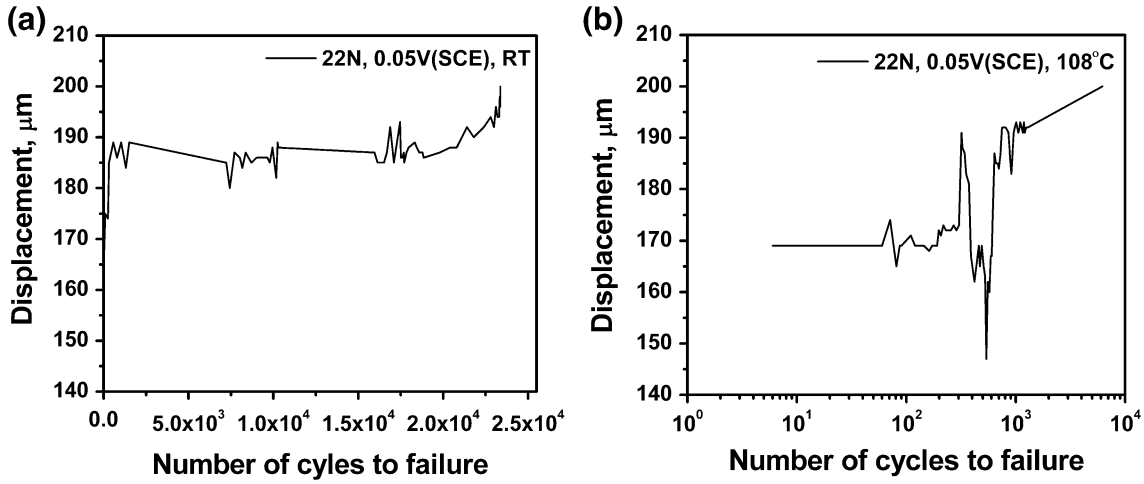

Fig. 10. Variation of strain displacement with the number of cycles to failure recorded during the CF test of Type 316LN SS with 0.22 wt.% nitrogen at a applied potential of 0.05 V (SCE) for a mean stress of 375 MPa at both (a) room-temperature and (b) boiling conditions.

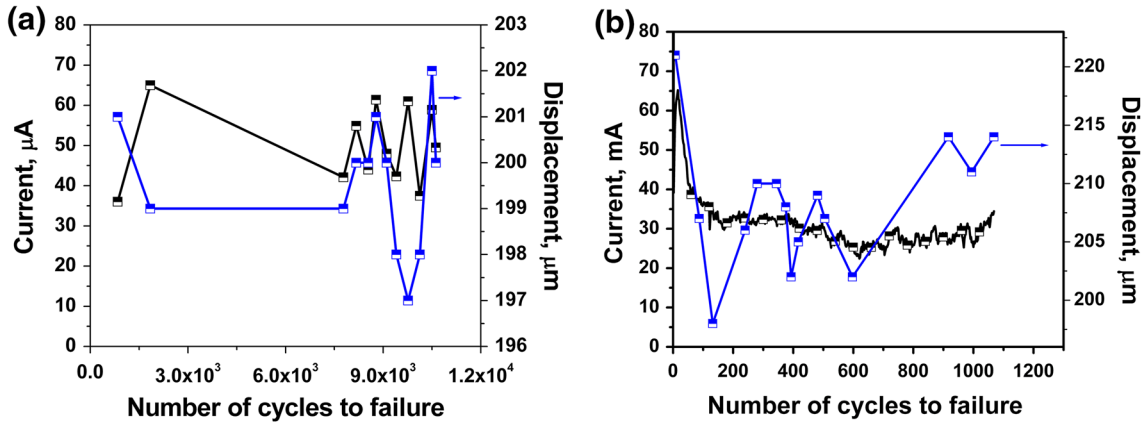

Fig. 11. Variation of strain displacement and current versus number of cycles to failure recorded during the CF test of Type 316LN SS with 0.07 wt.% nitrogen at a applied potential of 0.05 V (SCE) at (a) room-temperature and (b) boiling conditions.

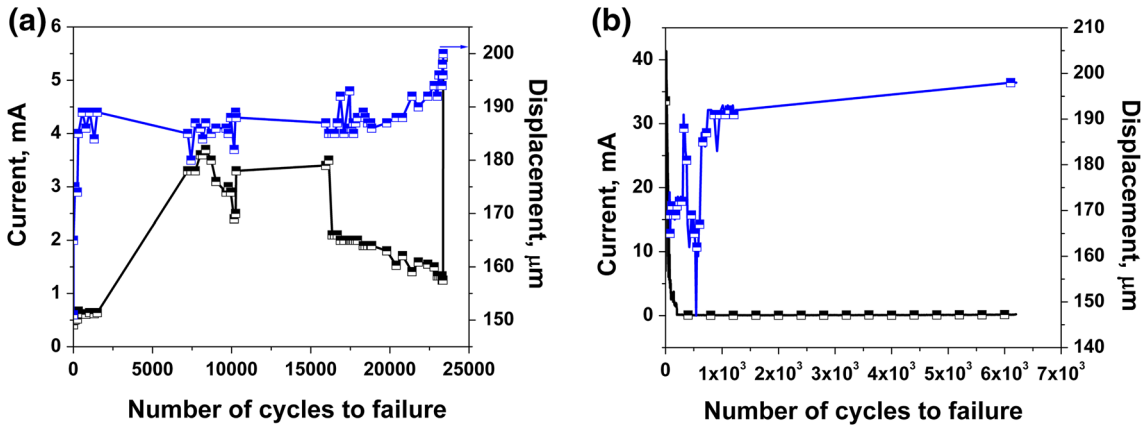

Fig. 12. Variation of strain displacement and current versus number of cycles to failure recorded during the CF test of Type 316LN SS with 0.22 wt.% nitrogen at an applied potential of 0.05 V at (a) room-temperature and (b) boiling conditions.

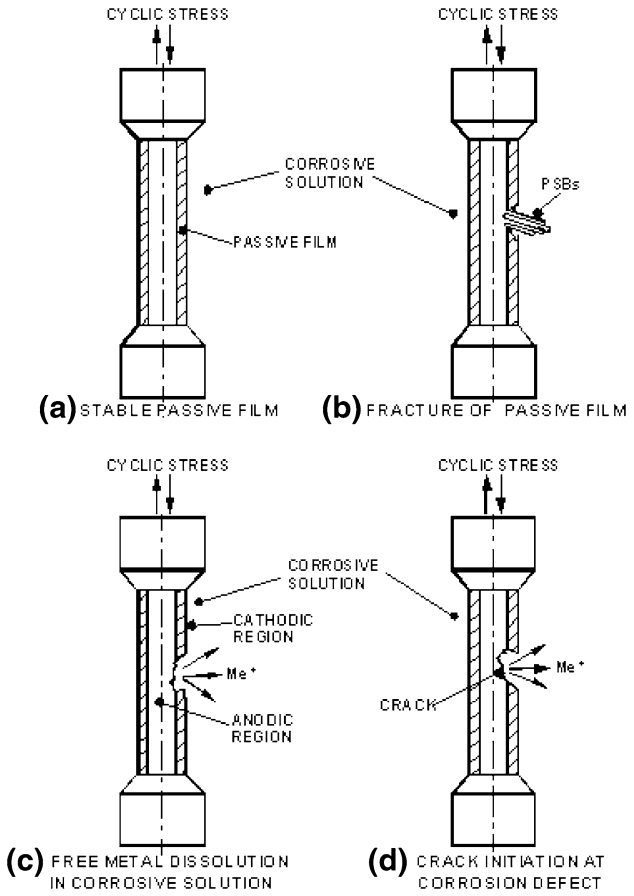

Fig. 13. Schematic of corrosion fatigue crack-initiation model.

Thereafter, strain displacement increased continuously, indicating crack growth, until final failure; although variation in the current amplitude was less, the magnitude of current amplitude was much higher, which signified accelerated crack growth. 316LN SS with 0.22 wt.% nitrogen showed increase in strain displacement at 16,000 cycles indicating the formation of microcracks in room-temperature studies (Fig. 12a). However, this process was found to be much faster in the boiling condition (Fig. 12b), as the strain displacement was found to rise after 600 cycles. The initial rise in current coinciding with the rise in the displacement was correlated to the damage or dissolution of the passive film, and recovery (repassivation) of the passive film was correlated to the constant displacement. Further increases in current and concurrent displacement were correlated to the microcracking process initiated at the pits, which are known to be the stress raisers. Once initiated, the microcracks were found to grow in a periodic manner due to active dissolution of the cracks followed by their repassivation. The process continued until final fracture.

The first schematic diagram in Fig. 13 shows the breakdown of the passive film during the application of the potential in the passive region. The application of cyclic load creates slip steps that emerge at the surface, resulting in the breakdown of the passive film at these spots. The process of repassivation and breakdown proceed continuously until the film can no longer repassivate, resulting in the microcrack from the surface flaws. The second illustration shows the process of film breakdown due to the initiation of metastable pits at the flaws

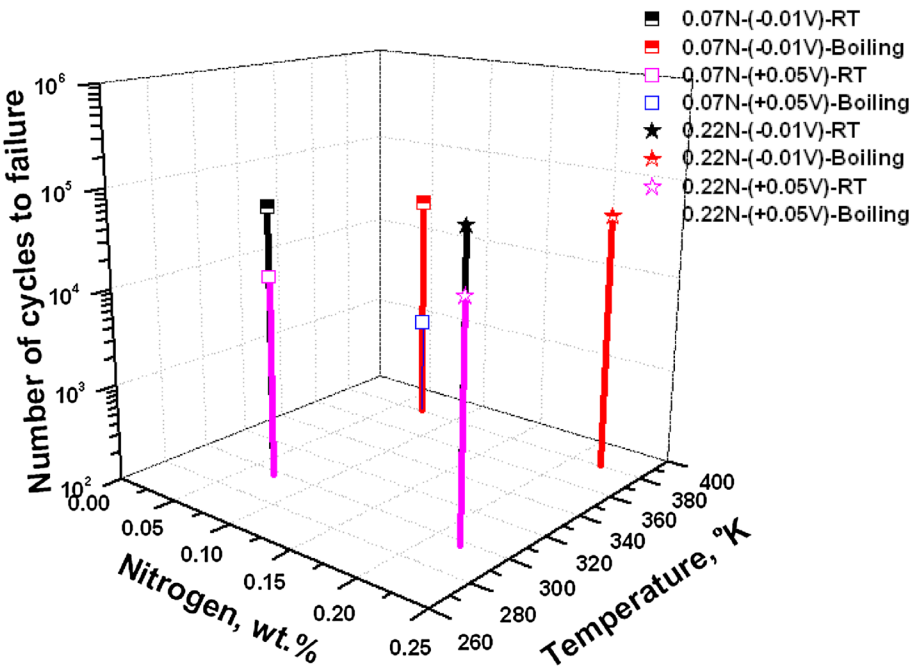

Fig. 14. Number of cycles to failure at different applied potential.

in the passive film. The cyclic load induces the flaws in the passive film, which in the presence of chloride ions promptly result in the metastable pits at these locations. The metastable pits grow in the conducive environment resulting in the formation of micro-cracks. These processes are accelerated when the temperature is increased, resulting in the failure of the specimen much faster than room-temperature tests. A schematic illustration of this CF process is illustrated in Fig. 13.

Figure 14 shows the number of cycles to failure for both nitrogen-containing specimens at room temperature and in the boiling condition at both applied potentials. The number of cycles to failure increased with a decrease in temperature. The effect of nitrogen is pronounced in the passive region at room temperature compared with the boiling condition. In the boiling condition, in the metastable corrosion region, the effect of nitrogen was found to be less, as the kinetics of the pitting corrosion reaction was much faster resulting in severe pitting, which accelerated the failure of the specimen. However, at room temperature, powerful effect of nitrogen could be observed. The mechanical depassivation that resulted from the cyclic load outweighs the electrochemical repassivation resulting from the environment during the final stages of the failure of the specimen. However, initial repassivation of the passive film results in much longer life of the specimen.

In connection with the above discussion, it could be recalled that nitrogen addition also produces beneficial effects of increasing the pitting corrosion resistance by suppressing the metastable pits, growing the existing pits, and facilitating the repassivation rate immediately after the breakdown of the passive film.[4] Metastable pit growth is a well-documented early stage in pitting corrosion of stainless steel in chloride solution. Metastable pitting can be observed as current excursions under potentiostatic control or distinct current transients during electrochemical noise (EN) studies.[44] Each metastable pitting event reflects the initiation, growth, and repassivation of a micropit. Metastable pit transients can be recorded at potentials below the pitting potential.

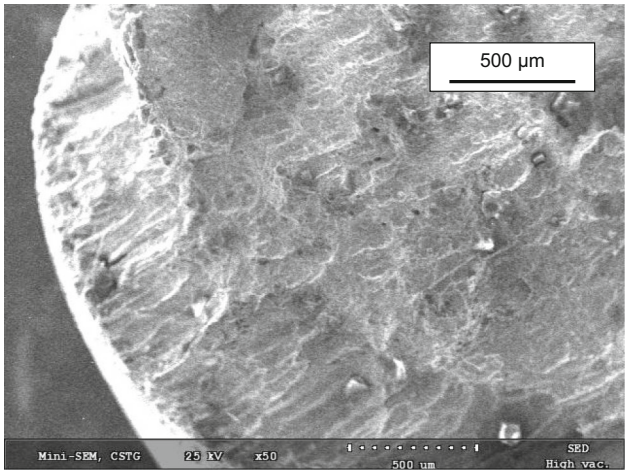

Fig. 15. Crack-initiation site in 0.07 wt.% nitrogen for corrosion fatigue in the acidified chloride solution.

Fractography

The fractured specimen surface was examined after CF testing. The SEM observations show that the fatigue cracks initiated at the corrosion defects on surface in all testing conditions as shown in Fig. 15. It is concluded that the corrosion effect (depassivation of the material) is not dependent solely on the chloride content in the environment, but the decrease in fatigue strength was also found to be equally important. The presence of $C1^-$ ions accelerated the growth rate tenfold over that in air; it also changed the type of fatigue striations formed. In air, the striations were evenly spaced ripples on the fracture surface. They are termed "ductile" striations because their overall appearance

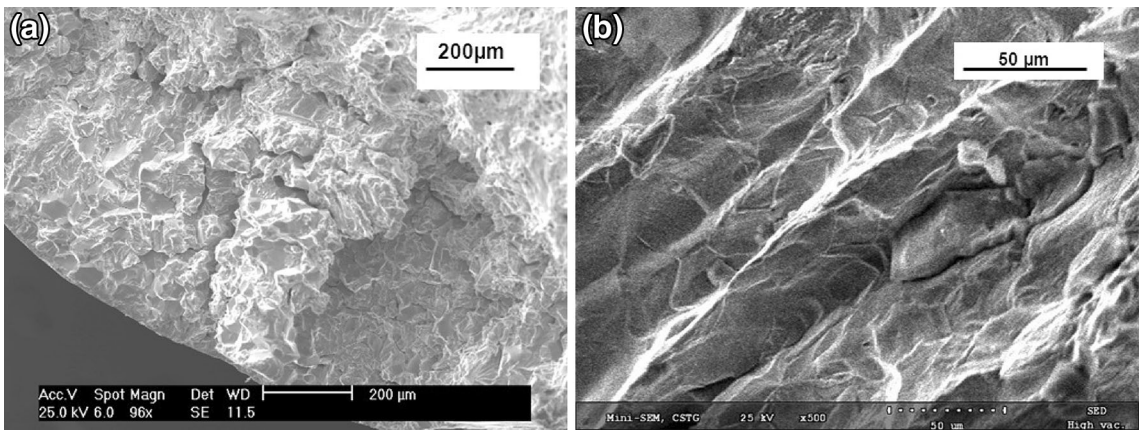

Fig. 16. Fracture surface showing (a) transgranular mode of fracture in 0.07 wt.% nitrogen and (b) "brittle" striations in 0.22 wt.% nitrogen containing steel after CF test.

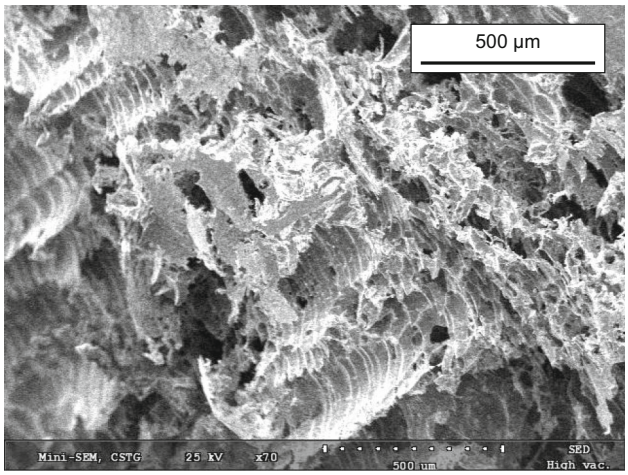

Fig. 17. Severe general corrosion on the specimen surfaces after corrosion fatigue test in the acidified chloride solution for 0.07 wt.% nitrogen at boiling conditions.

suggested a large amount of plastic blunting at the crack tip. On the other hand, "brittle" striations, which form in chloride solutions, are much more uneven in their appearance and have cleavage-like features as seen in Fig. 16a.[38] Under applied potential, cleavage facets, fragments of "river pattern" secondary cracks, running along the growth direction of the main crack appear on the fracture surface as shown in Fig. 16b.[45] At the applied potential of $-0.1V_{SCE}$, severe general corrosion was observed on the specimen surface at boiling condition as shown in Fig. 17.[35] The fatigue region can be easily identified by its relatively flat features compared with the dimpled fracture overload region surrounding it. Because of these large corrosion pits, fatigue crack initiation lives and fatigue crack initiation threshold stresses of the specimens in the boiling condition are significantly inferior to those of specimens exposed to room temperature.[46] The fracture surface observed in Fig. 16a and b showed that the cracking was wholly transgranular, and no switch over to the intergranular mode was observed.

CONCLUSION

1. Potentiodynamic anodic polarization behavior of 0.07 wt.% N steel showed the shift of the polarization diagram by several orders of magnitude of current density in the boiling acidified 1 M NaCl solution compared with that obtained at room temperature. There was no distinct active peak in the boiling condition and the specimen showed pseudo-passivity with very high passive current density values.
2. Unlike 0.07 wt.% N steel, 0.22 wt.% N steel showed the pitting potential to be about 0.0 V (SCE), and the current rose after E_{pp} drastically.
3. Applied potential in the region of metastable pitting enhanced the chances of formation of pits which induce microcracks resulting in the faster failure.
4. At room temperature, the effect of potential in the metastable pitting region clearly depicted the formation of microcracks at 7×10^3 cycles for 0.07 wt.% N, which could be visualized in the plots of displacement as well in current transients versus the number of cycles.
5. In the stable passive region, the specimen showed a lot of current fluctuations at both room-temperature and boiling conditions because of the dynamic depassivation–repassivation process.
6. The SEM observations showed that the fatigue cracks had initiated at surface defects under all testing conditions.

REFERENCES

1. B. Raj and U.K. Mudali, *High Nitrogen Stainless Steels* (New Delhi: Narosa Publishing House, 2004), p. 1.
2. U.K. Mudali and S. Ningshen, *Corrosion Properties of Nitrogen Bearing Stainless Steels, High Nitrogen Steels and SS* (New Delhi: Narosa Publishing House, 2004), p. 133.
3. U.K. Mudali, R.K. Dayal, J.B. Gnanamoorthy, and P. Rodriguez, *Mater. Trans. Jpn. Inst. Met.* 37, 1568 (1996).
4. A. Poonguzhali, M.G. Pujar, and U.K. Mudali, *J. Mater. Eng. Perform.* 22, 1170 (2013).
5. S.L. Mannan, S.C. Chetal, B. Raj, and S.B. Bhoje (Paper presented at the Proceedings of the Seminar on Materials R & D for PFBR, Kalpakkam, India, 2003).
6. R. Ebara (Paper presented at the Proceedings of the JSCE Materials and Environments, 1985), pp. 221–224.
7. R. Ebara, *Proc. Eng.* 2, 1297 (2010).
8. B. Baroux, *Further Insights on the Pitting Corrosion of Stainless Steels. Corrosion Mechanisms in Theory and Practice*, 2nd ed., ed. P. Marcus (New York: Marcel Dekker, 2002), p. 311.
9. Z. Smialowska-Szklarska, *Pitting Corrosion of Metals* (Houston, TX: NACE International, 1986), p. 430.
10. H.H. Strehblow, *Mechanisms of Pitting Corrosion*, *Corrosion Mechanisms in Theory and Practice*, ed., P. Marcus and J. Ouder (New York: Marcel Dekker, 2002), p. 243.
11. S. Ishihara, Z.Y. Nan, A.J. McEvily, T. Goshima, and S. Sunada, *Int. J. Fatigue* 30, 1659 (2008).
12. R. Ebara, *Mater. Sci. Eng. A* 468–470, 109 (2007).
13. H.M. Shalaby, J.A. Begley, and D.D. MacDonald, *Corrosion* 52, 262 (1996).
14. J. Xie, A.T. Alpas, and D.O. Northwood, *Mater. Charact.* 48, 271 (2002).
15. E. Rezig, P.E. Irving, and M.J. Robinson, *Proc. Eng.* 2, 387 (2010).
16. T. Magnin and I. Coudreuse, *Acta Metall.* 35, 2105 (1987).
17. I. Olefjord and L. Wegrelius, *Corros. Sci.* 38, 1203 (1996).
18. Y. Lu, R. Bandy, C.R. Clayton, and R.C. Newman, *J. Electrochem. Soc.* 130, 1774 (1983).
19. G. Okamoto (Paper presented at the Proceedings of the Conference on Passivity and Its Breakdown on Iron and Iron Base Alloys, Houston, TX, 1976) pp. 106–109.
20. A.T. Fromhold, *Oxides and Oxide Films,* vol. 4, ed. J.W. Diggle (New York: Marcel Dekker, 1976), pp. 1–271.
21. J. Bessone (Ph.D. Thesis, University of Manchester Institute of Science and Technology, 1983).
22. C. Escriva-Cerdana, E. Blasco-Tamarita, and D.M. Garcia-Garciaa, *Chem. Eng. Trans.* 32, 1717 (2013).
23. L.L. Shreir, R.A. Jarman, and G.T. Burstein, *Corrosion* (New York: Wiley, 2000).
24. B.R. Tzaneva, *Bulgarian Chem. Commun.* 46, 378 (2014).
25. H.Y. Ha, H. Jang, H.S. Kwon, and S. Kim, *Corros. Sci.* 51, 48 (2009).
26. U.K. Mudali, B. Reynders, and M. Stratmann, *Corros. Sci.* 41, 179 (1999).

27. Y. Fu, X. Wu, E.-H. Han, W. Ke, K. Yang, and Z. Jiang, *Electrochim. Acta* 54, 4005 (2009).
28. M. Kumagai, S.T. Myung, S. Kuwata, R. Aaishi, Y. Katada, and H. Yashiro, *Electrochim. Acta* 54, 1127 (2009).
29. C. Trépanier and A.R. Pelton (Paper presented at the Proceedings of the International Conference on Shape Memory and Superelastic Technologies, Kurhaus Baden-Baden, Baden-Baden, Germany, 3–7 October 2004).
30. R.F.A. Jargelius-Pettersson, *Corros. Sci.* 41, 1639 (1999).
31. R.C. Newman and W.R. Whitney, *Corrosion* 57, 1030 (2001).
32. Z. Begum, A. Poonguzhali, R. Paul, H. Shaikh, R.V. Subba Rao, A.K. Patil, and R.K. Dayal, *Corros. Sci.* 53, 1424 (2011).
33. U. Kamachi Mudali and Y. Katada, *Electrochim. Acta* 46, 3735 (2001).
34. Z.S. Tong, B.X. Feng, H.Q. Li, and Y. Shi, *Corrosion* 41, 121 (1985).
35. J.B. Duh, W.T. Tsai, J.T. Lee, and H. Chang, *Corrosion* 46, 983 (1990).
36. S. Degallaix, J.I. Dickson, and J. Foct, *Proceedings of the First International Conference on High Nitrogen Steels "HNS 88,"* eds. J. Foct and A. Hendry (London, U.K.: The Institute of Metals, 1989), p. 380.
37. J.W. Simmons, *J Mater. Sci. Eng. A* A207, 159 (1996).
38. R.M. Pelloux, R.E. Stoltz, and J.A. Moskovitz, *Mater. Sci. Eng.* 25, 193 (1976).
39. K. Hladky and J.L. Dawson, *Corros. Sci.* 22, 231 (1982).
40. T. Anita, M.G. Pujar, H. Shaikh, R.K. Dayal, and H.S. Khatak, *Corros. Sci.* 48, 2689 (2006).
41. C. Amzallag, B. Mayonobe, and P. Rabbe, *Electrochemical Corrosion Testing, ASTM STP/727,* eds. F. Mansfeld and U. Bertocci (West Conshohocken, PA: ASTM International, 1981), pp. 69–83.
42. R. Ebara, *Eng. Fail Anal.* 13, 516 (2006).
43. G. Greenfield, *Corrosion Fatigue: Chemistry, Mechanics and Microstructure* (Houston, TX: NACE International, 1972), p. 133.
44. M.G. Pujar, U.K. Mudali, and S. Sekar Singh, *Corros. Sci.* 53, 4178–4186 (2011).
45. S.A. Shiplov, *Environmentally Induced Cracking of Materials,* ed. S.A. Shiplov, R.H. Jones, J.M. Olive, and R.B. Rebak (New York: Elsevier Science Ltd., 2008).
46. P.S. Pao, S.J. Gill, and C.R. Feng, *Scripta Mater.* 43, 391 (2000).